Small RNA stabilization via non-covalent binding with a metalloporphyrin nanocage to accomplish synergistic gene and photodynamic therapy

Jin, Weiguang; Xin, Li; Veiga, Gael Clergeaud; Ray, Roslyn M.; Hong Lin, Marie Karen Tracy; Andresen, Thomas Lars; Gotfredsen, Charlotte Held; Nielsen, Martin; Astakhova, Kira; Qvortrup, Katrine

Published in:
Cell Reports Physical Science

Link to article, DOI:
10.1016/j.xcrp.2022.101187

Publication date:
2022

Document Version
Publisher's PDF, also known as Version of record

Cell Reports
Physical Science

CellPress
OPEN ACCESS

Article

Small RNA stabilization via non-covalent binding with a metalloporphyrin nanocage to accomplish synergistic gene and photodynamic therapy

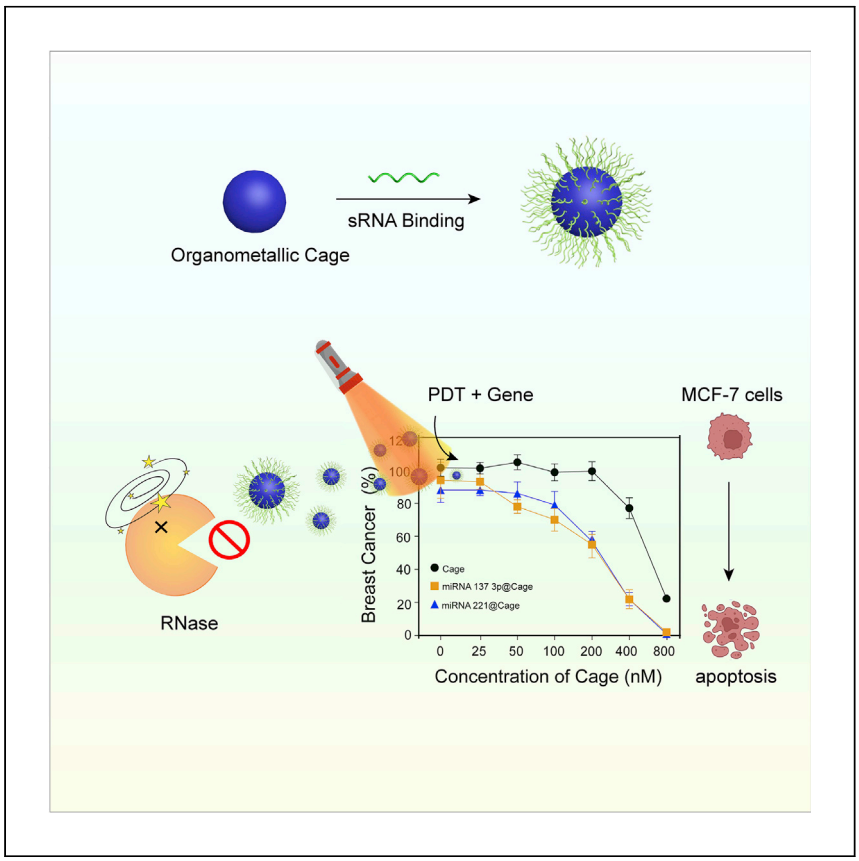

Small RNAs are regarded as attractive therapeutic agents, but biodegradation severely limits their application. Herein, Weiguang et al. report on small RNAs binding to metalloporphyrin cages, significantly protecting RNA against degradation and facilitating synergistic gene regulation and photodynamic therapy for killing breast cancer cells.

Weiguang Jin, Xin Li, Gael Clergeaud, ..., Martin Nielsen, Kira Astakhova, Katrine Qvortrup

kiraas@kemi.dtu.dk (K.A.)
kaqvo@kemi.dtu.dk (K.Q.)

Highlights

Small RNAs efficiently bind to metalloporphyrin cages via non-covalent interactions

Strong binding significantly enhances the small RNA human serum stability

The platform is used for synergistic gene regulation and photodynamic therapy

Jin et al., Cell Reports Physical Science 3, 101187
December 21, 2022
https://doi.org/10.1016/j.xcrp.2022.101187

Please cite this article in press as: Jin et al., Small RNA stabilization via non-covalent binding with a metalloporphyrin nanocage to accomplish synergistic gene and photodynamic therapy, Cell Reports Physical Science (2022), https://doi.org/10.1016/j.xcrp.2022.101187

Cell Reports
Physical Science

CellPress
OPEN ACCESS

Article

Small RNA stabilization via non-covalent binding with a metalloporphyrin nanocage to accomplish synergistic gene and photodynamic therapy

Weiguang Jin,[1] Xin Li,[2] Gael Clergeaud,[2] Roslyn M. Ray,[3] Marie Karen Tracy Hong Lin,[4] Thomas Lars Andresen,[2] Charlotte Held Gotfredsen,[1] Martin Nielsen,[1] Kira Astakhova,[1,*] and Katrine Qvortrup[1,5,*]

SUMMARY

Small RNAs (sRNAs) have emerged as attractive therapeutic agents due to their gene-editing and -regulatory properties. However, their application is severely limited by their relatively short circulation half-lives. Herein, we report a strategy binding sRNA with metalloporphyrin cages that leads to a significant protection of sRNA against RNase degradation and increased half-lives. Nuclear magnetic resonance (NMR) titration of nucleosides and nucleotides demonstrates that π-stacking and electrostatic interactions contribute to the sRNA binding, which occurs on the external surface of the nanocage. Moreover, the cage binding promotes sRNA internalization, and the sRNAs maintain genetic activity after release in an acidic intracellular environment. Taking advantage of the photodynamic properties of the cage, the nanosystem shows efficient *in vitro* cell killing through gene regulation and photodynamic effects, providing evidence for its therapeutic potential in breast cancer treatment. We envision the proposed strategy may provide new insight for the development of organometallic cage-based sRNA delivery vehicles.

INTRODUCTION

Small RNA (sRNA), defined as RNA with 18–30 nucleotides,[1] is therapeutically important for a range of human diseases, including cancer. In CRISPR-Cas9 gene editing, for example, the use of guide RNA (gRNA) functions as a guide for targeting enzymes, which is a key strategy to minimize off-target effects and optimize efficiency of the system.[2] In addition, endogenous sRNA molecules, such as microRNA (miRNA), have been linked to many diseases,[3] especially cancer,[4] as their biological action results in the overexpression of oncogenic proteins or the down-regulation of tumor-suppressor proteins.[5] Introducing exogenous miRNA that inhibit gene expression of overexpressed miRNA or balance down-regulated miRNA are promising gene therapies.[6] Therapeutic applications of sRNA are, however, severely limited due to their susceptibility to degradation by prevalent ribonucleases in the bloodstream and cell environment,[7] which results in short circulation half-lives of less than 2 min.[8] To overcome the instability of RNA, the use of RNA-loaded nanoparticles has received increasing attention due to their nanoscale size and functional surface.[9] A broad range of nanomaterials have been investigated, including metallic nanoparticles,[10] liposomes,[11] and polymers.[12]

Learning from the nanoparticle-RNA formulations, metal-organic cages (MOCs) are attractive nanocomponents for sRNA binding and stabilization due to their unique

[1]Department of Chemistry, Technical University of Denmark, 2800 Kongens Lyngby, Denmark

[2]Department of Health Technology, Technical University of Denmark, 2800 Kongens Lyngby, Denmark

[3]Center for Gene Therapy, City of Hope-Beckman Research Institute, Duarte, CA 91010, USA

[4]National Center for Nanofabrication and Characterization, Technical University of Denmark, 2800 Kongens Lyngby, Denmark

[5]Lead contact

*Correspondence: kiraas@kemi.dtu.dk (K.A.), kaqvo@kemi.dtu.dk (K.Q.)

https://doi.org/10.1016/j.xcrp.2022.101187

Please cite this article in press as: Jin et al., Small RNA stabilization via non-covalent binding with a metalloporphyrin nanocage to accomplish synergistic gene and photodynamic therapy, Cell Reports Physical Science (2022), https://doi.org/10.1016/j.xcrp.2022.101187

structural characteristics. Driven by self-assembly of molecular components, MOCs are rationally constructed as highly symmetrical and discrete supramolecular polyhedrons, which facilitate their nanoscale dimensional distribution.[13] In addition, these structurally well-defined MOCs allow the incorporation of desired functional groups to modify the structural characteristics, resulting in expeditious tuning of key features, including solubility as well as binding properties, with the ability to bind a wide range of guest molecules through relevant non-covalent interactions.[14] Meanwhile, intrinsic relatively weak and dynamic non-covalent host-guest supramolecular binding allows the convenient reattachment of guest molecules at a low energy cost.[15] Compared with the traditional metal complex, the MOCs arouse extensive interest in supramolecular host-guest interaction due to their large cavity and surface area.[16,17] Guest encapsulation using the interior cavity is the most popular strategy to explore and utilize the supramolecular binding ability of MOCs.[18,19] This interior binding generally needs a suitable internal environment within the cavity to match the desired trapped guest molecules.[20] While this is effective for the binding of small-molecule guests, it does not allow encapsulation and stabilization of larger biomolecules.[21–23] To further expand the application of MOCs, the binding of guest molecules to the exterior surface is an attractive strategy.[24,25] Ward and coworkers recently showed strong binding between anionic aromatic fluorophores and the exterior surface of cationic MOCs.[26]

Due to the above-mentioned advantages of host-guest interactions, the binding of DNA molecules with $Ni^{II}_4L_6$[27] and $Fe_4{}^{II}L_4$ tetrahedral cages[28,29] was recently reported, protecting DNA from nuclease-mediated degradation. Compared with DNA, reports describing sRNA binding with MOCs are limited. The higher instability of RNA compared with DNA, resulting from a nucleophilic attack on the phosphorus atom attacked by the adjacent ribose 2′ hydroxyl groups, pose a major challenge when designing RNA binders.[30] Given that DNA deoxynucleotides and RNA ribonucleotides are similar structural motifs, the pioneering DNA recognition studies offer a positive reflection to our proposal of sRNA binding and stabilization with MOCs.

Recent studies have shown that a combination of sRNA, especially miRNA, transfection, and photodynamic therapy (PDT) has a strong anti-cancer effect.[31–33] Various MOC-based nanostructures were utilized as photosensitizers to generate reactive oxygen species (ROS),[18] but, to our knowledge, there is no report on sRNA-bound MOC structures for sRNA stabilization, miRNA activity, and PDT. Given the strong properties of the porphyrin unit as a photosensitizer,[34] we hypothesized that a $Fe^{II}_8L_6$ metalloporphyrin structure could show strong sRNA binding and stabilization while having good anti-cancer properties through miRNA-mediated gene regulation and MOC-based PDT.

Herein, we present the preparation and characterization of two isostructural metalloporphyrin cubic cages (Scheme 1) and demonstrate their ability to bind sRNA, hereby significantly enhancing sRNA resistance against RNase degradation and stability in human serum. Nuclear magnetic resonance (NMR) titration of relevant nucleoside and nucleotide biomolecules demonstrate that electrostatic and π-stacking interactions contribute to the binding. The encapsulation of coronene inside the cage has a negligible effect on dinucleotide and sRNA binding, confirming that the binding only occurred on the external surface of the cage. Moreover, the bound sRNA can be released under acidic conditions, mimicking the cancer intracellular environment.

As a proof-of-concept study, we selected breast cancer MCF-7 cells to demonstrate that the cage significantly promoted the internalization of the bound sRNA and

Please cite this article in press as: Jin et al., Small RNA stabilization via non-covalent binding with a metalloporphyrin nanocage to accomplish synergistic gene and photodynamic therapy, Cell Reports Physical Science (2022), https://doi.org/10.1016/j.xcrp.2022.101187

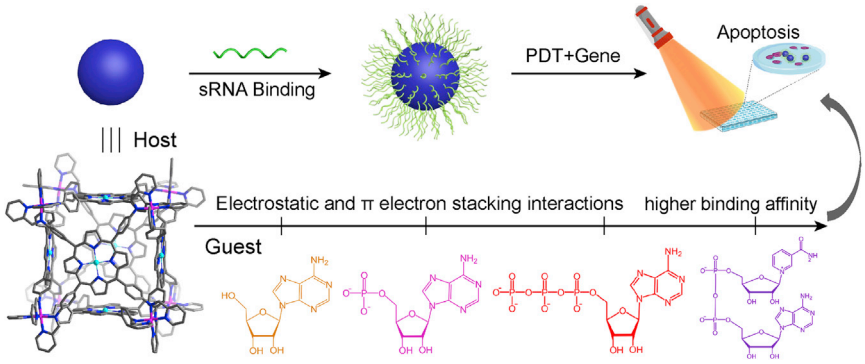

Scheme 1. Small RNA surface binding with metalloporphyrin cage through electrostatic and π-stacking interactions, resulting in significate stability against ribonuclease degradation and a synergistic therapy involving gene regulation and cage-based PDT for breast cancer treatment (cage 1·SO_4 contains zinc-porphyrin motifs, while its isostructural cage 2·SO_4 contains free-base porphyrin faces)

maintenance of its biological activity after release from the cage. Importantly, the sRNA@cage nanocomplex facilitated synergistic therapeutic behavior combining miRNA regulation and PDT properties, efficiently killing MCF-7 cells. Overall, our findings demonstrated the feasibility of reversible surface binding for the preparation of MOC-based sRNA carriers and their potential use as a synergistic enhancer for cancer therapies using a combination of gene regulation and PDT. We envision that the results may create new insight and inspiration for the use of MOC-based sRNA delivery vehicles.

RESULTS AND DISCUSSION

Characterization of the sRNA binding with cages

Cage 1·SO_4 and cage 2·SO_4 were synthesized through subcomponent self-assembly[35] (Section S2 in the supplemental experimental procedures) and, rewardingly, were found to display both good water solubility and stability under physiological conditions as seen from their time-dependent UV-visible (UV-vis) (Figure S8) and NMR (Figure S9) spectroscopy. In addition, dynamic light scattering (DLS) indicated that cages disperse at nanoscale in water (Figures S10 and S11). The ILK-1 CRISP gRNA, designed to knock out the integrin-linked kinase encoding gene,[36] was used for initial binding studies with equal concentrations of cage. The cationic cages 1·SO_4 and 2·SO_4 bound the innate negatively charged sRNA through electrostatic interactions, as the corresponding zeta potential of cages changed from positive to negative after mixing with equal concentrations of sRNA (Figure S12). Meanwhile, the single negative charge signal of complexes indicated that the sRNA was located on the external surface of the cages (Section S4 in the supplemental experimental procedures).[37] Efficient binding was also seen from ILK-1 titration, which induced a red shift of the UV-vis absorbance spectra of cage 1·SO_4 (Figure 1B).[38] When we extended the binding study to other sRNA, miRNA 221 and miRNA 137 3p, similar phenomena were seen in both zeta potentials and UV-vis absorbance (Sections S4 and S5 in the supplemental experimental procedures).

Denaturing PAGE was also used to study the binding. Since the positively charged cage acts as a counter ion to the negatively charged RNA, the intensity and mobility of the RNA bands on the gel will be affected by the cage concentration.[39] As shown in Figure 1C, the cage was not absorbed into the gel due to charge repulsion but instead was driven into the running buffer,[29] resulting in a black lane 1, while the

Please cite this article in press as: Jin et al., Small RNA stabilization via non-covalent binding with a metalloporphyrin nanocage to accomplish synergistic gene and photodynamic therapy, Cell Reports Physical Science (2022), https://doi.org/10.1016/j.xcrp.2022.101187

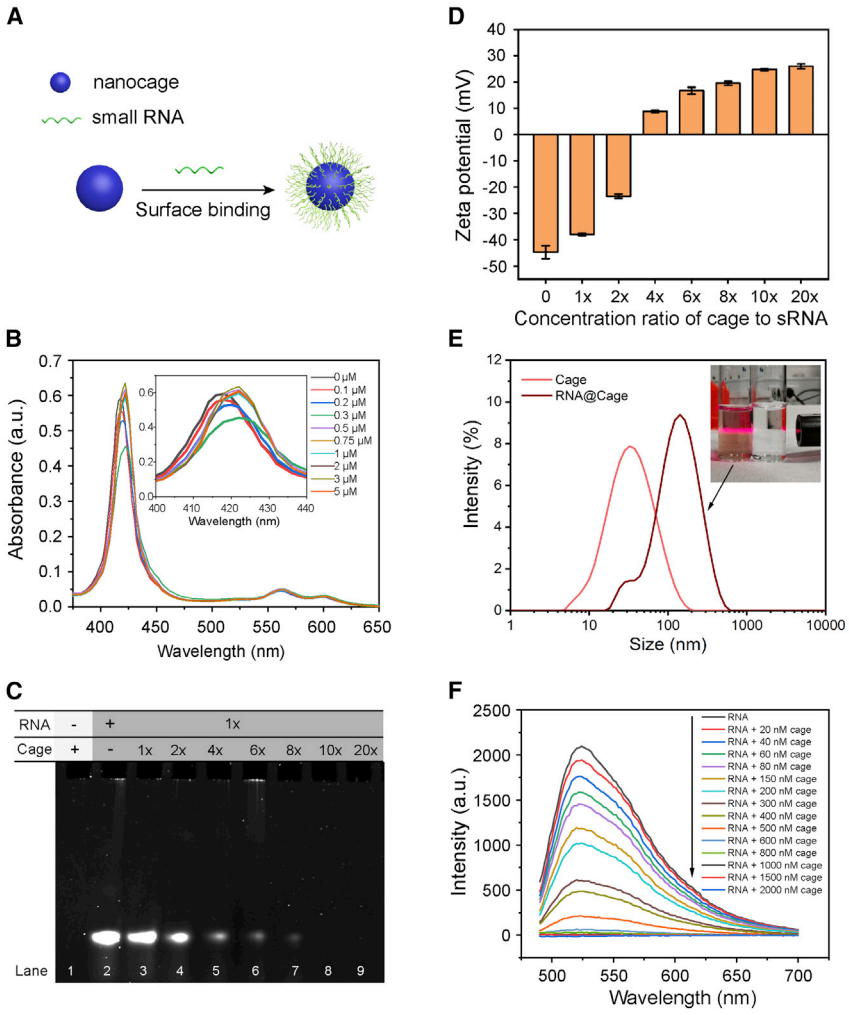

Figure 1. Characterization of the sRNA binding with cages

(A) Cartoon showing the formation of sRNA@cage.

(B) UV-vis absorbance spectra of cage 1·SO_4 with ILK-1 titration.

(C) PAGE image of naked cage 1·SO_4 (lane 1), naked miRNA 137 3p (lane 2), and the corresponding complexes of miRNA 137 3p@cage 1·SO_4 with various concentration ratios (lanes 3–9).

(D) Average zeta potential value of miRNA 137 3p without and with cage 1·SO_4 at various concentration ratios. The data are presented as means ± SDs (n = 3).

(E) DLS particle size distribution of bare cage 1·SO_4 and miRNA137 3p@cage 1·SO_4. The inserted picture shows the Tyndall effect of the miRNA137 3p@cage 1·SO_4 transparent brown solution (left), while nothing is observed in the water (right). The molar ratio of cage:RNA was kept at 10:1.

(F) Fluorescent quenching of 100 nM FAM-labeled ILK-1 dependent on cage 1·SO_4 concentration.

signal of naked miRNA 137 3p is seen in lane 2 upon applying the electrophoresis voltage. The corresponding PAGE band intensity of the complexes gradually decreased and disappeared when the cage concentration reached 10 equiv to miRNA 137 3p (Figure 1C, lane 8), which is ascribed to the zeta potential of mixtures gradually increasing and changing from negative to positive (Figure 1D), further indicating complete binding. The same gel phenomena were observed for ILK-1 and miRNA 221, where signals also disappeared in the presence of 10 equiv of cage (Figures S28 and S29). As expected, the binding increased the DLS particle size, and the complex formed a transparent suspension with typical Tyndall effect (Figure 1E). Both sRNA@cage 1·SO_4 and sRNA@cage 2·SO_4 showed negligible

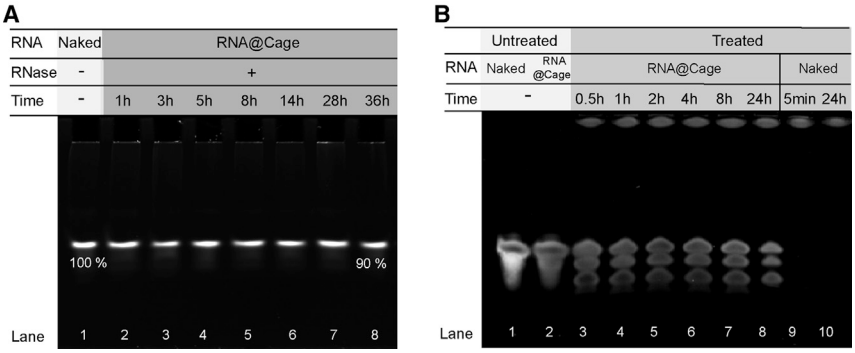

Figure 2. Cage binding enhances sRNA stability

RNA stability analyzed by PAGE measurement of miRNA 137 3p@cage 1·SO_4 incubated with RNase (A) and ILK-1 with or without cage 1·SO_4 in human serum (B) at different times (the concentration ratio of cage 1·SO_4 to RNA was kept as 10:1; the percentage of RNA was analyzed by the band intensity, while the naked RNA at lane 1 was used as reference).

changes in the time-dependent UV-vis spectra and the DLS particle size distribution over the course of 48 h, thereby demonstrating the stability of the complexes in solution (Figures S30 and S31). The transmission electron microscopy (TEM) image showed that the amorphous RNA was aggregated around the cage nanoparticles (Figure S32B), which could also confirm that the RNA was bound to the outer surface of the cage nanoparticles, although the vacuum drying measurement conditions resulted in the loss of morphology of sRNA@cage.

To gain more insights into the interaction, we studied the fluorescent behavior of the 6-carboxyfluorescein (FAM)-labeled sRNA under cage titration. The emission of FAM-sRNA can be effectively quenched by cage through fluorescence resonance energy transfer.[40] As shown in Figure 1F, an increase in the concentration of cage 1·SO_4 gradually weakened the fluorescence emission of the FAM-labeled ILK-1 gRNA and led to complete quenching with 10 equiv cage, which is consistent with PAGE binding rate. In addition, similar effects on the fluorescence were seen upon titration of cage 1·SO_4 with FAM-labeled miRNA 137 3p and cage 2·SO_4 with FAM-labeled ILK-1 (Figure S33). Importantly, no obvious fluorescent change of the free dye was observed when it was mixed with the cages (Figure S34A), and the respective components of the cages had no significant quenching effect on the FAM-RNA fluorescence (Figure S34B). These results clearly illustrate that the quenching originates from the interaction of the cage with the sRNA rather than with the FAM molecule and that only the fully assembled cage structures allow effective interaction.

Cage binding enhances sRNA stability

Encouraged by the binding behavior, we investigated the potential of the cage for sRNA stabilization via PAGE. As RNase is a common enzyme causing RNA hydrolysis in biological microenvironments,[41] we first evaluated the stability of sRNA with and without cage binding under RNase digestion. No PAGE band was observed from miRNA 137 3p after 1 h (Figure S36), which indicates complete degradation. On the contrary, the band corresponding to the miRNA 137 3p was well retained from the samples containing cage 1·SO_4 (Figure 2A), and approximately 90% of intact miRNA 137 3p was observed after 36 h. We further investigated the stability of sRNA in human serum. Notably, these experiments also showed a significant resistance to degradation of ILK-1 gRNA when complexed to the cage. The presence of intact ILK-1 could be observed after 24 h of exposure to serum, while the naked

Please cite this article in press as: Jin et al., Small RNA stabilization via non-covalent binding with a metalloporphyrin nanocage to accomplish synergistic gene and photodynamic therapy, Cell Reports Physical Science (2022), https://doi.org/10.1016/j.xcrp.2022.101187

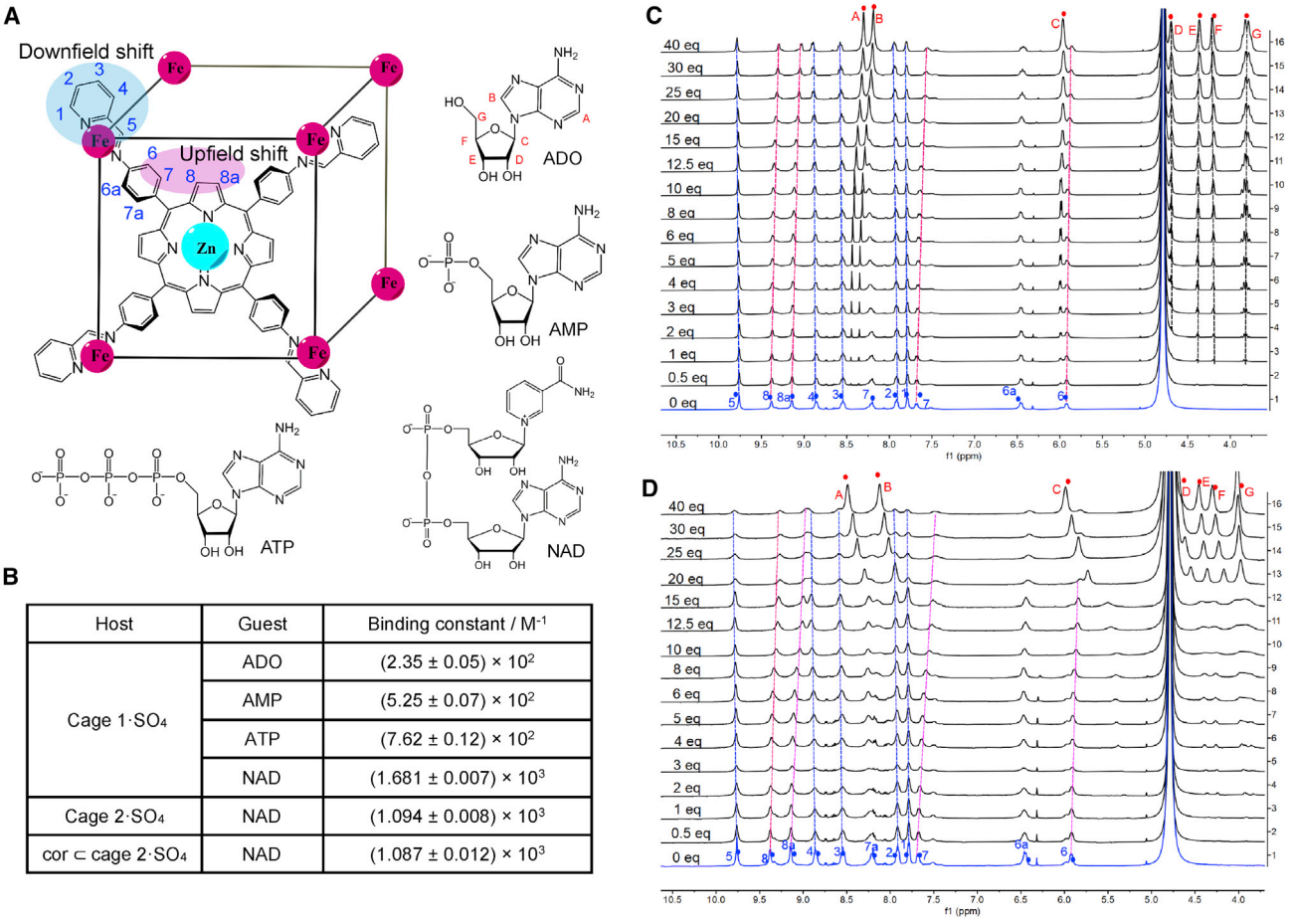

Host	Guest	Binding constant / M^{-1}
Cage 1·SO_4	ADO	(2.35 ± 0.05) × 10^2
	AMP	(5.25 ± 0.07) × 10^2
	ATP	(7.62 ± 0.12) × 10^2
	NAD	(1.681 ± 0.007) × 10^3
Cage 2·SO_4	NAD	(1.094 ± 0.008) × 10^3
cor ⊂ cage 2·SO_4	NAD	(1.087 ± 0.012) × 10^3

Figure 3. Binding mechanism investigated by nucleoside and nucleotide NMR titration

(A and B) The prospective nucleoside and nucleotide NMR titration (A) and their affinity constants with cages (B).

(C and D) The titration of ADO (C) and AMP (D) with cage 1·SO_4 monitored by ^{1}H NMR, respectively (blue and pink lines denote down-field and up-field shifts, respectively).

ILK-1 rapidly degraded within 5 min (Figures 2B, S37, and S38). These results clearly demonstrate that the cage has the ability to protect sRNA against RNase biodegradation and improve the stability in human serum.

Binding mechanism study

To explore the binding mechanism, selective nucleoside and nucleotide biomolecules were employed for NMR titration experiments (Figure 3A). Aliquots of cage 1·SO_4 were added to the respective biomolecule solution with different concentrations, and the corresponding spectra were recorded sequentially. Clear changes in chemical shift ($|\Delta\delta| > 0.01$ ppm) of proton resonances corresponding to both cage and guests were observed during titration, indicating that the cage can bind both nucleoside and nucleotide biomolecules.[42] Meanwhile, the corresponding calculated binding constants of the biomolecules illustrate their different affinity with cage (Figure 3B). Based on the ^{1}H NMR results of adenosine (ADO) titration (Figure 3C), the signals of nucleobase showed a gradual up-field shift, while the ribose remained unchanged during the titration. Meanwhile, the central porphyrin ring of the cage gradually shifted toward upfield, while an opposite trend occurred in the pyridine ring. Therefore, we speculated that there is a π-stacking interaction

Please cite this article in press as: Jin et al., Small RNA stabilization via non-covalent binding with a metalloporphyrin nanocage to accomplish synergistic gene and photodynamic therapy, Cell Reports Physical Science (2022), https://doi.org/10.1016/j.xcrp.2022.101187

between the ADO nucleobase and the central porphyrin component of the cage,[43] triggering an electron transfer from the terminal site of cage to its central part.

Cage 1·SO_4 also showed a change in chemical shift upon titration with ADO monophosphate (AMP), but the nucleotide behaved completely different compared with the ADO (Figure 3D). The signal of the ribose moiety experienced a gradual down-field shift, while signals remained unchanged in ADO, and the base unit shifted downfield. A significant $\Delta\delta$ (0.02–2.31 ppm) was observed in the ^{31}P NMR titration spectrum of AMP (Figure S44), and its significantly higher association affinity demonstrated that the phosphate also participates in the interaction, which led to its different ^{1}H NMR behavior compared with ADO. This proposed interaction was confirmed by studying the binding between ADO triphosphate (ATP) and cage 1·SO_4. Similarly, all signals of the ATP guest undergo a down-field shift in both ^{1}H NMR and ^{31}P NMR spectra (Figures S46 and S47). Moreover, the cage 1·SO_4 exhibited a higher binding affinity for ATP compared with AMP (Figure S48).

To further verify this speculative mechanism, the complexation of nicotinamide adenine dinucleotide (NAD) was studied. As expected, all signals of NAD gradually shifted downfield (Figure S49), and the binding constants indicate that cage 1·SO_4 binds NAD with high affinity (Figure S50). When replacing cage 1·SO_4 with cage 2·SO_4, the same interaction with NAD was observed (Figure S51). The only difference between these two interactions is that the binding coefficient of cage 1·SO_4 is higher than that of cage 2·SO_4 (Figure S52), which reinforces the hypothesis that electrostatic interactions dominate the binding, as cage 1·SO_4 has a higher positive electron potential compared with cage 2·SO_4. Moreover, the ^{1}H NMR signals of cage 2·SO_4 also showed a gradual up-field shift in central porphyrin ring along with a down-field shift in its terminal pyridine, which occurred in the ^{1}H NMR of cage 1·SO_4 with all selected nucleoside and nucleotide biomolecules, further demonstrating that a similar π-stacking interaction occurred. Therefore, the two main interactions that contribute to the cage-sRNA binding are concluded to be π stacking between sRNA unpaired base units and the central porphyrin of the cage as well as electrostatic interactions between the negatively charged sRNA and the positively charged cage, with our experiments indicating that the latter dominates the binding.

Verification of outside surface binding

To confirm that the biomolecule is bound to the outer surface of the cage structure instead of entering its cavity, we introduced a coronene molecule into the cage 2·SO_4 to fill its cavity, forming cor⊂cage 2·SO_4 (Section S12 in the supplemental experimental procedures). Coronene was chosen as a relevant model structure due to its electrical neutrality in addition to the previously reported successful encapsulation of coronene in cage 2·OTf.[44] Afterward, NMR titration experiments were performed with biomolecule NAD and cor⊂cage 2·SO_4 in an aqueous solution to identify whether the coronene affects the nucleotide binding (Figure 4A). Although the cavity was occupied, the result of ^{1}H NMR was similar to studies of the empty cage 2·SO_4, with an insignificant change in binding affinity (Figure S55). Meanwhile, the encapsulated coronene showed an up-field shift arising from the higher shielding effect induced by the NAD binding on the external surface of cage, indicating the coronene maintained inside the cage during the nucleotide binding.

In addition to the NMR titration experiment, we also performed a fluorescence assay to investigate the interaction between cor⊂cage 2·SO_4 and FAM-labeled sRNA to evaluate the effect of coronene encapsulation on sRNA binding. Similar to the empty

Please cite this article in press as: Jin et al., Small RNA stabilization via non-covalent binding with a metalloporphyrin nanocage to accomplish synergistic gene and photodynamic therapy, Cell Reports Physical Science (2022), https://doi.org/10.1016/j.xcrp.2022.101187

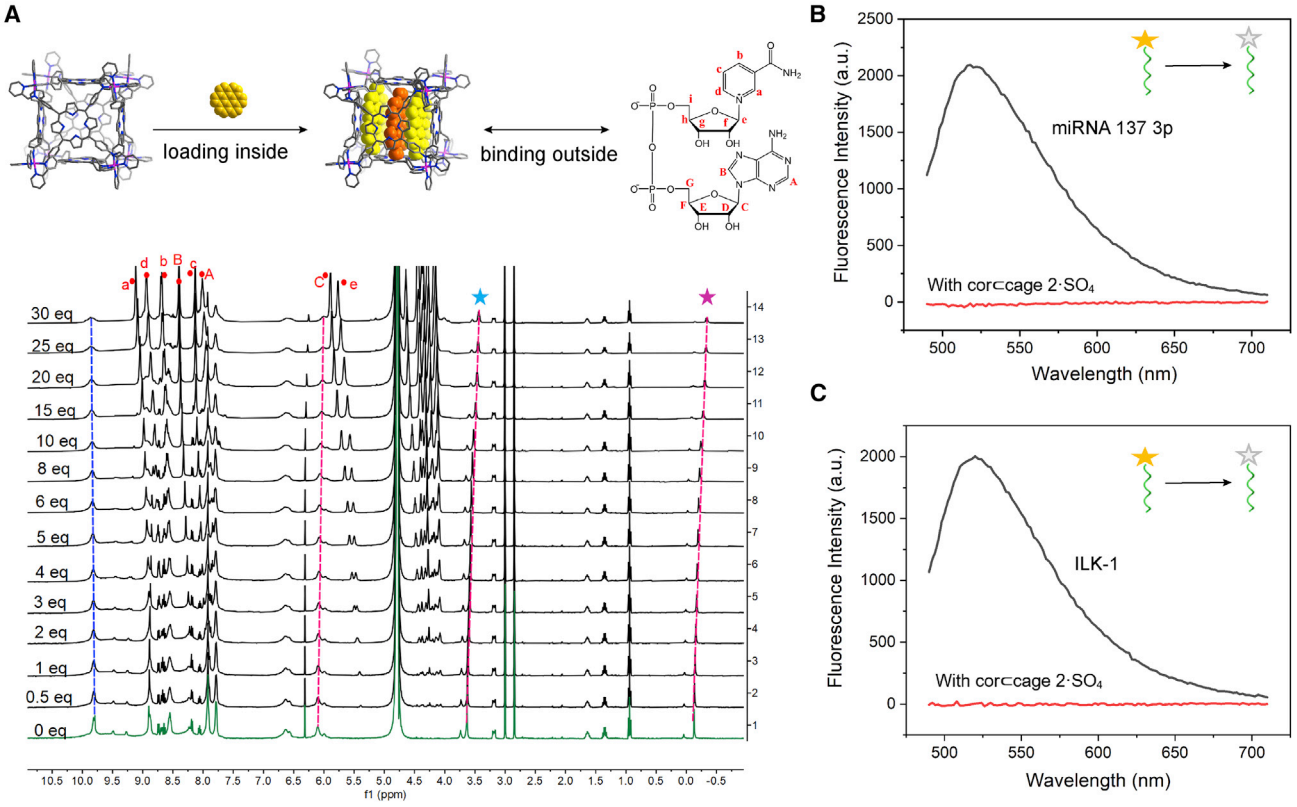

Figure 4. Verification of sRNA binding with the outside surface of cage

(A) NAD nucleotide NMR titration with cor⊂cage 2·SO_4 (blue and pink lines denote down-field and up-field shifts, respectively; the signal of trapped coronene, which is marked with blue and pink stars, experience gradual up-field shift during the titration).

(B and C) The complex of cor⊂cage 2·SO_4 led to fluorescence quench of FAM-labeled miRNA 137 3p (B) and FAM-labeled ILK-1 sequences (C).

cage, the FAM-labeled miRNA 137 3p and ILK-1 were quenched by cor⊂cage 2·SO_4, respectively, indicating that the encapsulation of coronene has negligible effects on sRNA binding (Figures 4B and 4C). Given that the RNA sequence has a significantly larger molecular size than NAD, this also indicates that the bound RNA was located on the outer surface of the cage. According to the fact that sRNA only interacts with the exterior surface of the cage, we can conclude successful surface binding. Meanwhile, we also envision that the unexplored interior cavity could be used for other small-molecule deliveries, which will be investigated in the future.

RNA release

As sRNA has been proven to bind the exterior surface of the cage through non-covalent host-guest supramolecular binding, we next studied the sRNA release properties. The miRNA 137 3p@cage 2·SO_4 (ratios: 1:5 and 1:10) complexes were incubated in both neutral and acidic aqueous solutions (pH 5) for 1 h, followed by PAGE analysis. As shown in Figure 5A, the PAGE signal (lanes 4–7) of the intact miRNA 137 3p was clearly observed after incubation in acidic solution, mimicking the acidic intracellular environment of cancer. This demonstrates that the miRNA 137 3p can be released from the cage in an acidic environment. In contrast, when incubated with up to 10 equiv of the cage in neutral buffer (lane 3), no band corresponding to released sRNA was observed. These results also demonstrate retained strong RNA and cage binding under neutral conditions, which mimic circulating conditions. EDTA

Please cite this article in press as: Jin et al., Small RNA stabilization via non-covalent binding with a metalloporphyrin nanocage to accomplish synergistic gene and photodynamic therapy, Cell Reports Physical Science (2022), https://doi.org/10.1016/j.xcrp.2022.101187

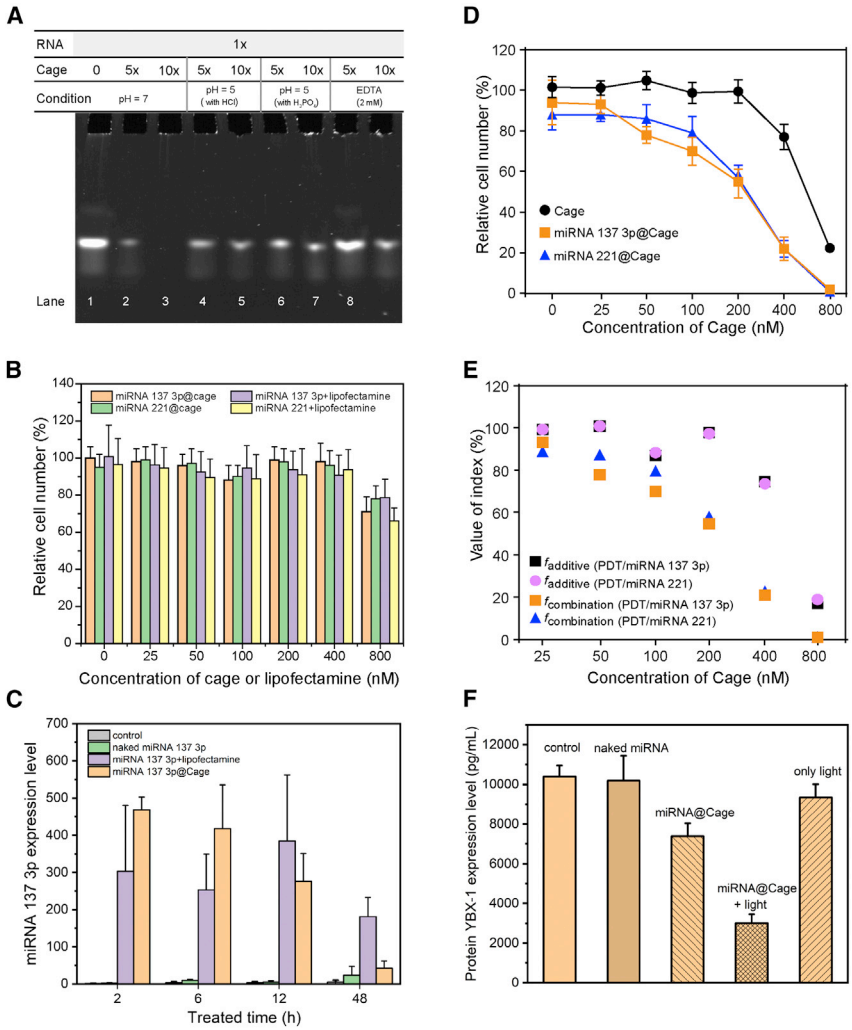

Figure 5. RNA release and the synergistic gene regulation and photodynamic effect for therapeutic potential in breast cancer treatment

(A) The release of miRNA 137 3p from the complex of miRNA 137 3p@ cage 2·SO_4 measured by PAGE (the naked miRNA 137 3p at lane 1 is used as reference).

(B) Cytotoxicity of miRNAs with lipofectamine and miRNA@cage 2·SO_4 in MCF-7 cells at various concentrations for 48 h in the dark. The concentration ratio of lipofectamine:RNA or cage:RNA was 10:1. The data are presented as means ± SDs (n = 3).

(C) miRNA 137 3p level inside MCF-7 cells after treatment with different samples, which were prepared with the same miRNA amount with 10 equiv of lipofectamine or cag 2·SO_4. The data are presented as means ± SDs (n = 3).

(D) Cytotoxicity of cage 2·SO_4 and miRNA@cage 2·SO_4 in MCF-7 cells with light irradiation at various concentrations. The cells were exposed to a 416 nm wavelength light for 30 min during the 48 h treatment period, and the molar ratio of cage:RNA was maintained at 10:1. The data are presented as means ± SDs (n = 3).

(E) Compared with the $f_{additive}$, the significantly smaller $f_{combination}$ at various concentrations indicates a synergistic gene regulation and photodynamic effect of miRNA@cage 2·SO_4.

(F) Protein YBX-1 expression in the MCF-7 cells after treatment. The concentration of miRNA 137 3p was kept at the same for all sample preparations. The data are presented as means ± SDs (n = 3).

was also found to facilitate the RNA release (lanes 8 and 9). Also, exposing the miRNA 221@cage 2·SO_4 to acidic conditions promoted the release of miRNA 221 from the corresponding binding complex (Figure S56). We attribute disassembly of the cage in the acidic environment to impair sRNA binding, leading to sRNA release.[29]

Please cite this article in press as: Jin et al., Small RNA stabilization via non-covalent binding with a metalloporphyrin nanocage to accomplish synergistic gene and photodynamic therapy, Cell Reports Physical Science (2022), https://doi.org/10.1016/j.xcrp.2022.101187

MCF-7 cancer cell treatment

Having provided evidence for the release mechanism, we examined the potential of the sRNA@cage 2·SO_4 in cancer treatment. Considering that miRNA 221 and miRNA 137 3p are involved in the genetic dysregulation in breast cancer,[45,46] we studied MCF-7 cell viability with naked miRNA 137 3p, miRNA 221, and their respective cage complexes. After 48 h incubation in the dark, no obvious cytotoxicity was observed from naked miRNAs at various concentrations (Figure S57), which was ascribed to miRNA degradation and inefficient intracellular transfection. In contrast, a slight reduction in cell count was observed in the presence of miRNA 221@cage 2·SO_4 and miRNA 137 3p@cage 2·SO_4 (Figure 5B), which was highly similar to the data from the corresponding miRNAs transfected with lipofectamine, a commercial transfection reagent. To confirm that the cage can promote miRNA internalization, qPCR was performed to quantify the amount of miRNA 137 3p after treatment of MCF-7 cells with miRNA, miRNA transfected with lipofectamine, and miRNA 137 3p@cage 2·SO_4, respectively, at 2, 6, 12, and 48 h (Figure 5C). After 2 h treatment, no miRNA 137 3p was found in the cell treated with naked miRNA, but a significate miRNA amount was detected when miRNA 137 3p was transfected with both lipofectamine and cage 2·SO_4. The miRNA 137 3p@cage 2·SO_4 transfected the highest amount of RNA at 2 h, with a gradual decrease of miRNA 137 3p levels observed over treatment time, which may be attributed to the release of bound RNA and subsequent relevant biodegradation in the cancer cells. The gradual decreasing trend of the RNA amount with transfection time was also observed when using lipofectamine. Rewardingly, these findings clearly demonstrate that cage binding can efficiently enhance the cellular uptake of RNA and retain the biological activity of the RNA. In addition, no anti-proliferation effect was observed in healthy control cells, human dermal fibroblasts (HDFs), after 48 h incubation with cage 2·SO4 and the complexes (Figure S58), which reveals their biocompatibility.

Given the organic porphyrin component of the cage is a highly effective photosensitizer, the synergistic effect of PDT and the gene-regulating effect was studied for miRNA 221@cage 2·SO_4 and miRNA 137 3p@cage 2·SO_4. The cage was found to be stable under light irradiation at a 416 nm wavelength as the signal of cage 2·SO_4 in NMR and UV-vis spectra remained unchanged (Figures S59 and S60). Meanwhile, the generation of ROS was detected in cage 2·SO_4 and its miRNA complex solution under irradiation, showing their potential PDT properties (Figure S61). The cytotoxicity assay of MCF-7 cells with the treatment of cage 2·SO_4 and the miRNA complexes were applied to assess the synergistic therapy. As shown as Figure 5D, cage 2·SO_4 induced MCF-7 cell death with an IC_{50} value of 563.6 nM. Importantly, miRNA 221@cage 2·SO_4 and miRNA 137 3p@cage 2·SO_4 showed a significant enhanced cellular apoptosis, leading to full cell death at 800 nM. Their respective IC_{50} values were estimated as 204.8 and 178.5 nM. Comparing their additive index ($f_{additive}$), the respective smaller combination index ($f_{combination}$) clearly shows a synergistic effect of the gene regulation and PDT (Figure 5E).

To further understand the synergistic effect of PDT and miRNA gene regulation, we studied the expression of the potential targeted protein using enzyme-linked immunosorbent assay (ELISA). MCF-7 cells were treated with naked miRNA 137 3p, miRNA 137 3p@cage 2·SO_4, or miRNA 137 3p@cage 2·SO_4 with 30 min 416 nm light irradiation. Also, a control with only light irradiation was included. Restoring miRNA 137 3p expression is reported to inhibit the overexpression of target Y-box binding protein 1 (YBX1) and suppress cancer growth;[46,47] thus, we compared the expression level of YBX1 after 48 h treatment. As shown as Figure 5F, due to the lack of protection and transfection, the naked miRNA was unable to affect the YBX1

expression, with no apparent difference compared with untreated MCF-7 cells. In contrast, a reduction of the YBX1 expression was observed with miRNA 137 3p@cage $2{\cdot}SO_4$, further demonstrating that the RNA retained activity after cage binding. Importantly, better inhibition of protein expression was observed with miRNA 137 3p@cage $2{\cdot}SO_4$ with 30 min light irradiation, while the only light irradiation condition led to a negligible down-regulation of YBX1 expression as well as no decrease in cell viability in HDF and MCF-7 cells (Figure S62). These results show that the PDT of the cages and the miRNA activity give rise to a decrease in the expression of YBX1 in a synergistic manner to kill the MCF-7 cells. While the synergistic anti-cancer effect of the PDT and gene therapy have been previously reported,[48–52] it is notable that our work shows, for the first time, the combination of PDT and miRNA gene regulation of a sRNA@cage nanocomplex, thus expanding its potential biological application.

The above findings clearly demonstrate the ability of $Fe^{II}_8L_6$ cages to strongly bind sRNA through non-covalent interactions, significantly enhancing the stability of the sRNA against RNase degradation in serum. Importantly, only the fully assembled cages were found to effectively bind sRNA, as no significant interaction was seen with its structural components. The binding mechanism was investigated by NMR titration with relevant biomolecules, showing that the cage interacts with sRNA through a combination of π-stacking and electrostatic interactions, which is consistent with the structural characteristics of the cage consisting of a highly π-electron-dense and positively charged framework. The encapsulation of coronene inside the cage has a negligible effect on dinucleotide and sRNA binding, proving that the sRNA only binds the outer surface of the cage. Moreover, the cage binding promoted the sRNA internalization, while the bound sRNA maintained activity after release in the acidic intracellular environment. Using biologically relevant miRNA sequences, the potential of the cage as a synergistic treatment, combining gene regulation and PDT, was demonstrated in MCF-7 breast cancer cells. Encouraged by these results, we envision that the proposed surface binding strategy through non-covalent chemistry can be generalized to MOCs for sRNA delivery regardless of interior pore, which allows other small-molecule loading for co-delivery. We also believe that the presented MOC-based nanostructure provides new insight for the development of MOC-based sRNA delivery vehicles and new promising candidates for synergistic gene regulation and photodynamic tumor therapy.

EXPERIMENTAL PROCEDURES

Resource availability

Lead contact

Further information and requests for resources should be directed to and will be fulfilled by the lead contact, Katrine Qvortrup (kaqvo@kemi.dtu.dk).

Materials availability

This study did not generate new unique materials. Requests for any materials used in the manuscript are available from the lead contact upon reasonable request.

Data and code availability

Correspondence and requests for materials or data used in the manuscript are available from the lead contact upon reasonable request.

SUPPLEMENTAL INFORMATION

Supplemental information can be found online at https://doi.org/10.1016/j.xcrp.2022.101187.

ACKNOWLEDGMENTS

We are grateful to the China Scholarship Council for scholarship grant to W.J. (201808440383).

AUTHOR CONTRIBUTIONS

K.A. and K.Q. conceived the project; W.J. designed and performed the experiments; X.L. conducted the cytotoxicity assay; W.J. and X.L. analyzed data; R.M.R. conducted qPCR; M.K.T.H.L. measured the TEM imaging; C.H.G. provided expertise and feedback for NMR experiments; G.C., T.L.A., M.N., K.A., and K.Q. provided resources; W.J. and K.Q. drafted the manuscript; and all authors edited this manuscript.

DECLARATION OF INTERESTS

The authors declare no competing interests.

INCLUSION AND DIVERSITY

We support inclusive, diverse, and equitable conduct of research.

Received: July 11, 2022
Revised: October 19, 2022
Accepted: November 17, 2022
Published: December 8, 2022

REFERENCES

1. Ebhardt, H.A., Tsang, H.H., Dai, D.C., Liu, Y., Bostan, B., and Fahlman, R.P. (2009). Meta-analysis of small RNA-sequencing errors reveals ubiquitous post-transcriptional RNA modifications. Nucleic Acids Res. *37*, 2461–2470. https://doi.org/10.1093/nar/gkp093.

2. Jamal, M., Khan, F.A., and Da, L. (2016). Keeping CRISPR/Cas on-target. Curr. Issues Mol. Biol. *20*, 1–12. https://doi.org/10.21775/cimb.020.001.

3. Paul, P., Chakraborty, A., Sarkar, D., Langthasa, M., Rahman, M., Bari, M., Singha, R.K.S., Malakar, A.K., and Chakraborty, S. (2018). Interplay between miRNAs and human diseases. J. Cell. Physiol. *233*, 2007–2018. https://doi.org/10.1002/jcp.25854.

4. Peng, Y., and Croce, C.M. (2016). The role of microRNAs in human cancer. Signal Transduct. Target. Ther. *1*, 161–179. https://doi.org/10.1038/sigtrans.2015.4.

5. Hata, A., and Lieberman, J. (2015). Dysregulation of microRNA biogenesis and gene silencing in cancer. Sci. Signal. *8*, re3. https://doi.org/10.1126/scisignal.2005825.

6. Rooij, E., and Kauppinen, S. (2014). Development of micro RNA therapeutics is coming of age. EMBO Mol. Med. *6*, 851–864. https://doi.org/10.15252/emmm.201100899.

7. Houseley, J., and Tollervey, D. (2009). The many pathways of RNA degradation. Cell *136*, 763–776. https://doi.org/10.1016/j.cell.2009.01.019.

8. Baudrimont, A., Voegeli, S., Viloria, E.C., Stritt, F., Lenon, M., Wada, T., Jaquet, V., and Becskei, A. (2017). Multiplexed gene control reveals rapid mRNA turnover. Sci. Adv. *3*, e1700006. https://doi.org/10.1126/sciadv.1700006.

9. Boca, S., Gulei, D., Zimta, A.A., Onaciu, A., Magdo, L., Tigu, A.B., Ionescu, C., Irimie, A., Buiga, R., and Berindan-Neagoe, I. (2020). Nanoscale delivery systems for microRNAs in cancer therapy. Cell. Mol. Life Sci. *77*, 1059–1086. https://doi.org/10.1007/s00018-019-03317-9.

10. Hao, L., Patel, P.C., Alhasan, A.H., Giljohann, D.A., and Mirkin, C.A. (2011). Nucleic acid-gold nanoparticle conjugates as mimics of microRNA. Small *7*, 3158–3162. https://doi.org/10.1002/smll.201101018.

11. Maroof, H., Islam, F., Dong, L., Ajjikuttira, P., Gopalan, V., McMillan, N., and Lam, A. (2018). Liposomal delivery of miR-34b-5p induced cancer cell death in thyroid carcinoma. Cells *7*, 265. https://doi.org/10.3390/cells7120265.

12. Lopez-Bertoni, H., Kozielski, K.L., Rui, Y., Lal, B., Vaughan, H., Wilson, D.R., Mihelson, N., Eberhart, C.G., Laterra, J., and Green, J.J. (2018). Bioreducible polymeric nanoparticles containing multiplexed cancer stem cell regulating miRNAs inhibit glioblastoma growth and prolong survival. Nano Lett. *18*, 4086–4094. https://doi.org/10.1021/acs.nanolett.8b00390.

13. Ma, X., and Zhao, Y. (2015). Biomedical applications of supramolecular systems based on host-guest interactions. Chem. Rev. *115*, 7794–7839. https://doi.org/10.1021/cr500392w.

14. Ward, M.D., Hunter, C.A., and Williams, N.H. (2018). Coordination cages based on Bis(pyrazolylpyridine) ligands: structures, dynamic behavior, guest binding, and catalysis. Acc. Chem. Res. *51*, 2073–2082. https://doi.org/10.1021/acs.accounts.8b00261.

15. Liu, K., Kang, Y., Wang, Z., and Zhang, X. (2013). 25th Anniversary article: reversible and adaptive functional supramolecular materials: "noncovalent interaction" matters. Adv. Mater *25*, 5530–5548. https://doi.org/10.1002/adma201302015.

16. Jin, W.G., Chen, W., Xu, P.H., Lin, X.W., Huang, X.C., Chen, G.H., Lu, F., and Chen, X.M. (2017). An exceptionally water stable metal–organic framework with amide-functionalized cages: selective CO_2/CH_4 uptake and removal of antibiotics and dyes from water. Chem. Eur J. *23*, 13058–13066. https://doi.org/10.1002/chem.201701884.

17. Gosselin, E.J., Rowland, C.A., and Bloch, E.D. (2020). Permanently microporous metal-organic polyhedra. Chem. Rev. *120*, 8987–9014. https://doi.org/10.1021/acs.chemrev.9b00803.

18. Sepehrpour, H., Fu, W., Sun, Y., and Stang, P.J. (2019). Biomedically relevant self-assembled metallacycles and metallacages. J. Am. Chem. Soc. *141*, 14005–14020. https://doi.org/10.1021/jacs.9b06222.

19. Samanta, S.K., and Isaacs, L. (2020). Biomedical applications of metal organic polygons and polyhedra (MOPs). Coord. Chem. Rev. *410*, 213181. https://doi.org/10.1016/j.ccr.2020.213181.

20. Alimi, L.O., Alyami, M.Z., Chand, S., Baslyman, W., and Khashab, N.M. (2021). Coordination-based self-assembled capsules (SACs) for protein, CRISPR-Cas9, DNA and RNA delivery.

Chem. Sci. *12*, 2329–2344. https://doi.org/10.1039/d0sc05975g.

21. Rizzuto, F.J., von Krbek, L.K.S., and Nitschke, J.R. (2019). Strategies for binding multiple guests in metal–organic cages. Nat. Rev. Chem *3*, 204–222. https://doi.org/10.1038/s41570-019-0085-3.

22. Ronson, T.K., League, A.B., Gagliardi, L., Cramer, C.J., and Nitschke, J.R. (2014). Pyrene-edged FeII 4L6 cages adaptively reconfigure during guest binding. J. Am. Chem. Soc. *136*, 15615–15624. https://doi.org/10.1021/ja507617h.

23. Ronson, T.K., Meng, W., and Nitschke, J.R. (2017). Design principles for the optimization of guest binding in aromatic-paneled FeII4L6 cages. J. Am. Chem. Soc. *139*, 9698–9707. https://doi.org/10.1021/jacs.7b05202.

24. Sgarlata, C., Mugridge, J.S., Pluth, M.D., Tiedemann, B.E.F., Zito, V., Arena, G., and Raymond, K.N. (2010). External and internal guest binding of a highly charged supramolecular host in water: deconvoluting the very different thermodynamics. J. Am. Chem. Soc. *132*, 1005–1009. https://doi.org/10.1021/ja9056739.

25. Stelson, A.C., Hong, C.M., Groenenboom, M.C., Little, C.A.E., Booth, J.C., Orloff, N.D., Bergman, R.G., Raymond, K.N., Schwarz, K.A., Toste, F.D., et al. (2019). Measuring ion-pairing and hydration in variable charge supramolecular cages with microwave microfluidics. Commun. Chem. *2*, 1–10. https://doi.org/10.1038/s42004-019-0157-9.

26. Ludden, M.D., and Ward, M.D. (2021). Outside the box: quantifying interactions of anions with the exterior surface of a cationic coordination cage. Dalt. Trans. *50*, 2782–2791. https://doi.org/10.1039/d0dt04211k.

27. Xi, S.F., Bao, L.Y., Xu, Z.L., Wang, Y.X., Ding, Z.D., and Gu, Z.G. (2017). Enhanced stabilization of G-quadruplex DNA by [Ni4L6] 8+ cages with large rigid aromatic ligands. Eur. J. Inorg. Chem. *2017*, 3533–3541. https://doi.org/10.1002/ejic.201700409.

28. Zhu, J., Haynes, C.J.E., Kieffer, M., Greenfield, J.L., Greenhalgh, R.D., Nitschke, J.R., and Keyser, U.F. (2019). FeII4L4 tetrahedron binds to nonpaired DNA bases. J. Am. Chem. Soc. *141*, 11358–11362. https://doi.org/10.1021/jacs.9b03566.

29. Zhu, J., Yan, Z., Bošković, F., Haynes, C.J.E., Kieffer, M., Greenfield, J.L., Wang, J., Nitschke, J.R., and Keyser, U.F. (2021). Fe4II LL4tetrahedron binds and aggregates DNA G-quadruplexes. Chem. Sci. *12*, 14564–14569. https://doi.org/10.1039/d1sc04430c.

30. Fabre, A.L., Colotte, M., Luis, A., Tuffet, S., and Bonnet, J. (2014). An efficient method for long-term room temperature storage of RNA. Eur. J. Hum. Genet. *22*, 379–385. https://doi.org/10.1038/ejhg.2013.145.

31. Li, K., Zhang, Y., Hussain, A., Weng, Y., and Huang, Y. (2021). Progress of photodynamic and RNAi combination therapy in cancer treatment. ACS Biomater. Sci. Eng. *7*, 4420–4429. https://doi.org/10.1021/acsbiomaterials.1c00765.

32. Chakrabarti, M., Banik, N.L., and Ray, S.K. (2013). Photofrin based photodynamic therapy and miR-99a transfection inhibited FGFR3 and PI3K/Akt signaling mechanisms to control growth of human glioblastoma in vitro and in vivo. PLoS One *8*, e55652. https://doi.org/10.1371/journal.pone.0055652.

33. Kong, F., Zou, H., Liu, X., He, J., Zheng, Y., Xiong, L., and Miao, X. (2020). miR-7112-3p targets PERK to regulate the endoplasmic reticulum stress pathway and apoptosis induced by photodynamic therapy in colorectal cancer CX-1 cells. Photodiagnosis Photodyn. Ther. *29*, 101663. https://doi.org/10.1016/j.pdpdt.2020.101663.

34. Zhang, X., Wasson, M.C., Shayan, M., Berdichevsky, E.K., Ricardo-Noordberg, J., Singh, Z., Papazyan, E.K., Castro, A.J., Marino, P., Ajoyan, Z., et al. (2021). A historical perspective on porphyrin-based metal–organic frameworks and their applications. Coord. Chem. Rev. *429*, 213615. https://doi.org/10.1016/j.ccr.2020.213615.

35. Percástegui, E.G., Mosquera, J., and Nitschke, J.R. (2017). Anion exchange renders hydrophobic capsules and cargoes water-soluble. Angew. Chem. Int. Ed. *56*, 9136–9140. https://doi.org/10.1002/anie.201705093.

36. Zheng, C.-C., Hu, H.-F., Hong, P., Zhang, Q.-H., Xu, W.W., He, Q.-Y., and Li, B. (2019). Significance of integrin-linked kinase (ILK) in tumorigenesis and its potential implication as a biomarker and therapeutic target for human cancer. Am. J. Cancer Res. *9*, 186–197.

37. Alsaiari, S.K., Patil, S., Alyami, M., Alamoudi, K.O., Aleisa, F.A., Merzaban, J.S., Li, M., and Khashab, N.M. (2018). Endosomal escape and delivery of CRISPR/Cas9 genome editing machinery enabled by nanoscale zeolitic imidazolate framework. J. Am. Chem. Soc. *140*, 143–146. https://doi.org/10.1021/jacs.7b11754.

38. Brenner, W., Ronson, T.K., and Nitschke, J.R. (2017). Separation and selective formation of fullerene adducts within an MII8L6 cage. J. Am. Chem. Soc. *139*, 75–78. https://doi.org/10.1021/jacs.6b11523.

39. Gyi, J.I., Gao, D., Conn, G.L., Trent, J.O., Brown, T., and Lane, A. (2003). The solution structure of a DNA·RNA duplex containing 5-propynyl U and C; comparison with 5-Me modifications. Nucleic Acids Res. *31*, 2683–2693. https://doi.org/10.1093/nar/gkg356.

40. Yu, K., Wei, T., Li, Z., Li, J., Wang, Z., and Dai, Z. (2020). Construction of molecular sensing and logic systems based on site-occupying effect-modulated MOF-DNA interaction. J. Am. Chem. Soc. *142*, 21267–21271. https://doi.org/10.1021/jacs.0c10442.

41. Zhao, H., Li, T., Yao, C., Gu, Z., Liu, C., Li, J., and Yang, D. (2021). Dual roles of metal-organic frameworks as nanocarriers for miRNA delivery and adjuvants for chemodynamic therapy. ACS Appl. Mater. Interfaces *13*, 6034–6042. https://doi.org/10.1021/acsami.0c21006.

42. Plajer, A.J., Percástegui, E.G., Santella, M., Rizzuto, F.J., Gan, Q., Laursen, B.W., and Nitschke, J.R. (2019). Fluorometric recognition of nucleotides within a water-soluble tetrahedral capsule. Angew. Chem. Int. Ed. *58*, 4200–4204. https://doi.org/10.1002/anie.201814149.

43. Phongtongpasuk, S., Paulus, S., Schnabl, J., Sigel, R.K.O., Spingler, B., Hannon, M.J., and Freisinger, E. (2013). Binding of a designed anti-cancer drug to the central cavity of an RNA three-way junction. Angew. Chem. Int. Ed. *52*, 11513–11516. https://doi.org/10.1002/anie.201305079.

44. Meng, W., Breiner, B., Rissanen, K., Thoburn, J.D., Clegg, J.K., and Nitschke, J.R. (2011). A self-assembled M8L6 cubic cage that selectively encapsulates large aromatic guests. Angew. Chem. Int. Ed. *50*, 3479–3483. https://doi.org/10.1002/anie.201100193.

45. Nurzadeh, M., Naemi, M., and Sheikh Hasani, S. (2021). A comprehensive review on oncogenic miRNAs in breast cancer. J. Genet. *100*, 15. https://doi.org/10.1007/s12041-021-01265-7.

46. Zhu, X., Li, Y., Shen, H., Li, H., Long, L., Hui, L., and Xu, W. (2013). MiR-137 restoration sensitizes multidrug-resistant MCF-7/ADM cells to anticancer agents by targeting YB-1. Acta Biochim. Biophys. Sin. *45*, 80–86. https://doi.org/10.1093/abbs/gms099.

47. Johnson, T.G., Schelch, K., Cheng, Y.Y., Williams, M., Sarun, K.H., Kirschner, M.B., Kao, S., Linton, A., Klebe, S., McCaughan, B.C., et al. (2018). Dysregulated expression of the MicroRNA miR-137 and its target YBX1 contribute to the invasive characteristics of malignant pleural mesothelioma. J. Thorac. Oncol. *13*, 258–272. https://doi.org/10.1016/j.jtho.2017.10.016.

48. Borgia, F., Custurone, P., Peterle, L., Pioggia, G., Guarneri, F., and Gangemi, S. (2021). Involvement of micrornas as a response to phototherapy and photodynamic therapy: a literature review. Antioxidants *10*, 1–11. https://doi.org/10.3390/antiox10081310.

49. Piasecka, D., Braun, M., Kordek, R., Sadej, R., and Romanska, H. (2018). MicroRNAs in regulation of triple-negative breast cancer progression. J. Cancer Res. Clin. Oncol. *144*, 1401–1411. https://doi.org/10.1007/s00432-018-2689-2.

50. Kushibiki, T. (2010). Photodynamic therapy induces microRNA-210 and -296 expression in HeLa cells. J. Biophot. *3*, 368–372. https://doi.org/10.1002/jbio.200900082.

51. Guo, Q., Dong, B., Nan, F., Guan, D., and Zhang, Y. (2016). 5-Aminolevulinic acid photodynamic therapy in human cervical cancer via the activation of microRNA-143 and suppression of the Bcl-2/Bax signaling pathway. Mol. Med. Rep. *14*, 544–550. https://doi.org/10.3892/mmr.2016.5248.

52. El-Daly, S.M., Abba, M.L., and Gamal-Eldeen, A.M. (2017). The role of microRNAs in photodynamic therapy of cancer. Eur. J. Med. Chem. *142*, 550–555. https://doi.org/10.1016/j.ejmech.2017.10.011.